Energy & Environmental Science

Cite this: DOI: 10.1039/c2ee22657j

www.rsc.org/ees

COMMUNICATION

Enhancement of low energy sunlight harvesting in dye-sensitized solar cells using plasmonic gold nanorods†

Shuai Chang, Quan Li, Xudong Xiao, King Young Wong and Tao Chen*

Received 26th June 2012, Accepted 29th August 2012
DOI: 10.1039/c2ee22657j

This communication describes the use of Ag_2S-encapsulated Au nanorods (AuNR@Ag_2S) to enhance longer wavelength sunlight utility in dye-sensitized solar cells (DSSCs). We observed that the longitudinal plasmon resonance of AuNRs induces a remarkable increase of 37.6% in photocurrent generation at 600–720 nm. Optical characterizations indicate that the increased optical density and decreased light transmission as a result of AuNRs incorporation engender the striking improvement. With AuNR@Ag_2S, the final power conversion efficiency (PCE) of the DSSC with a thin anode (6 μm) increases from 4.3% to 5.6%, which is comparable to that of a pure TiO_2 anode based DSSC (5.8%) with a film thickness of 11 μm. Further, incorporation of AuNR@Ag_2S into the thick anode leads to the PCE increasing to 7.1%.

A dye-sensitized solar cell (DSSC) is composed of an inorganic semiconducting photoanode with adsorbed dye sensitizers and filled by electrolyte, and a platinized counter electrode.[1,2] This device configuration has attracted increasing interest primarily due to its easy fabrication and reasonably high solar-to-electric power conversion efficiency (PCE).[3–6] Extending the response of dye sensitizers to a broader range of the solar spectrum is a key step in further improving the device efficiency.[1,7] It is estimated that a PCE over 15% using I^-/I_3^- as redox couple would require a DSSC absorbing 80% of sunlight from 350 to 900 nm.[8] To date, the most efficient conventional sensitizers are polypyridyl ruthenium dyes with a bandgap of about 1.8 eV, *e.g.*, N3 and N719. Their strong absorption peaked at 530 nm while the absorption coefficient drastically decreased at longer wavelength.[1] Therefore, strategies that can increase the lower energy sunlight harvesting would maximize the usage of the existing dyes, leading to improved device efficiency. A few methods have been performed to extend the absorption spectrum through reorienting thiocyanate ligands, altering bipyridyl ligands, or replacing ruthenium with osmium as central metal.[8] Whereas light-to-electricity conversion at longer wavelengths is improved, the overall efficiency is not increased due to reduced light harvesting efficiency at the original absorption maximum. Other relevant works incorporate energy relay dyes[9] or develop new dye molecules with strong absorption in the red or near-infrared (NIR) region, such as those of indolines, coumarins and squaraines.[8,10–12] Nonetheless, the overall PCEs are usually smaller, sometimes becoming much lower, than those of N3/N719 analogues due to either loss of the strong absorption at 500–600 nm or difficulty in generating appropriate electronic configurations that match well with the semiconducting photoanode and/or tri-iodide electrolyte.[8,12] Apparently, increasing the photocurrent generation at longer wavelength of the conventional N3/N719 without sacrificing the original absorption is highly preferable.

A recently developed method to increase light utility in solar cells exploits localized surface plasmon (LSP) of noble metal nanostructures (*e.g.* Au, Ag).[13–15] By proper incorporation of metal

Department of Physics, The Chinese University of Hong Kong, Shatin, Hong Kong, China. E-mail: taochen@phy.cuhk.edu.hk; Fax: +86 852 2603 5204; Tel: +86 852 3943 6278

† Electronic supplementary information (ESI) available. See DOI: 10.1039/c2ee22657j

Broader context

Noble metal nanoparticles have demonstrated strong ability in light engineering. Surface plasmon resonance (SPR) of metal nanoparticles can effectively trap light to increase sunlight utility in solar cells. This communication reports the improvement of low energy sunlight harvesting in dye-sensitized solar cells using Au nanorods with longitudinal plasmon absorption maximum at 685 nm. We found that by proper incorporation of Ag_2S-encapsulated Au nanorods into a TiO_2 based photoanode, photocurrent generation at longer wavelengths (600–720 nm) can be enhanced by 37.6%. Since most of the conventional dyes or quantum dots show rapidly decreased absorption coefficients at longer wavelengths, the use of plasmon induced light trapping would find wide applications in enhancing solar spectrum response of the solar cells. Further, the SPR of metal nanoparticles dependent on the nanoscale morphology of the metal nanoparticle offers a unique platform for enhancing light harvesting at a specific wavelength and thus could be complementary to the development of dye molecules. This approach to increase the specific range of light utility would also be applicable for other photovoltaic devices such as polymer solar cells and inorganic thin film solar devices.

nanoparticles into electrodes, light can be efficiently trapped/concentrated as a result of surface plasmon resonance (SPR). The enhanced electric near-field and increased optical path length have demonstrated ability to improve the photocurrent density in silicon, GaAs and polymer solar cells.[15–18] To explore the potentials in DSSCs, most of the studies make use of SPR of spherical Ag or Au nanoparticles, but the photocurrent enhancement is usually restricted to around 430 nm and 530 nm, respectively.[13,19–23] Rod-like Ag and Au nanostructures have longitudinal plasmon absorption that can be tuned from visible, NIR and to the IR region by simply manipulating the aspect ratios of the rod,[24–26] providing a unique opportunity for utilizing the low energy range of the solar spectrum. Taking the stability and ease of synthesis into account, herein we use Au nanorods (AuNRs) to improve photocurrent generation in DSSCs.

It is noted that metallic nanoparticles are good conductors and often serve as recombination sites for photogenerated charge carriers. Therefore, the surfaces of the metallic nanoparticles are usually coated with a layer of TiO_2 or SiO_2 materials before incorporating into a DSSC. Such surface encapsulation also reduces the corrosion of metal nanoparticles by electrolyte, especially for Ag.[22] Hydrolysis of titanium or silicon precursors for the formation of the TiO_2 or SiO_2 shell has been widely used for the coating.[19,21] Nevertheless, AuNRs were synthesized using cationic surfactant hexadecyltrimethylammonium bromide (CTAB) as a morphology controlling surfactant forming double-layered CTAB (Fig. 1a and b).[26,27] Due to the long aliphatic tail of CTAB, it is difficult to coat a thin and dense layer of TiO_2 and SiO_2 by direct hydrolysis. Therefore, we encapsulate the AuNRs surface with a layer of Ag_2S *via* a two-step chemical process (Fig. 1a). The Ag shell firstly grows on the AuNRs surface through reduction of Ag^+ by ascorbic acid (see ESI† for details). This process can be easily carried out and the shell thicknesses are readily controlled by adding different amounts of $AgNO_3$. The Ag shell is thus transformed to Ag_2S by reacting with Na_2S,[28] and the final Ag_2S-coated AuNR is denoted as AuNR@Ag_2S (Fig. 1a and c). The thicknesses of Ag_2S are controlled at 2, 3.7 and 6.0 nm for investigations (Fig. 1c and S1†). The longitudinal absorption peak of AuNR@Ag_2S is at ~685 nm (2 nm shell thickness) (Fig. 1d), where the relatively strong irradiance of sunlight at this region ensures efficient SPR. At the same time, the absorption of N719 at around 685 nm is weak, thus the incorporation of AuNR@Ag_2S is expected to enhance sunlight harvesting in this range.

To obtain an optimized device performance, "plasmonic pastes" of TiO_2 nanoparticles containing AuNR@Ag_2S at different concentrations were prepared. A reference device was fabricated using only TiO_2 as anode material (device **1**). Fig. 2 shows the short-circuit current density (J_{sc}), open-circuit voltage (V_{oc}) characteristics; the J_{sc}, V_{oc} and PCE (η) of device **1** are measured to be 8.79 mA cm^{-2}, 0.726 V and 4.3%, respectively. With the incorporation of AuNR@Ag_2S (0.88% wt, device **2**), the PCE slightly increased to 4.5%. These device parameters are tabulated in Table 1 for easy comparison. The control experiment shows that the addition of AuNRs in the absence of Ag_2S leads to a PCE of 3.6% (Fig. S2†); the conducting Au surface can trap both electrons and holes and thus can serve as recombination sites. When the concentration of AuNR@Ag_2S reaches 1.69% wt (device **3**), PCE is further increased to 5.6% with J_{sc} and V_{oc} being 11.10 mA cm^{-2} and 0.786 V (Fig. 2 and Table 1). It can be seen that the enhancement in both V_{oc} and J_{sc} is responsible for the improved PCE. Since the conduction band of Ag_2S (−3.6 eV *vs.* E_{vac}) is more positive than that of TiO_2 (−4.2 eV *vs.* E_{vac}, Fig. S3†),[29,30] the charge

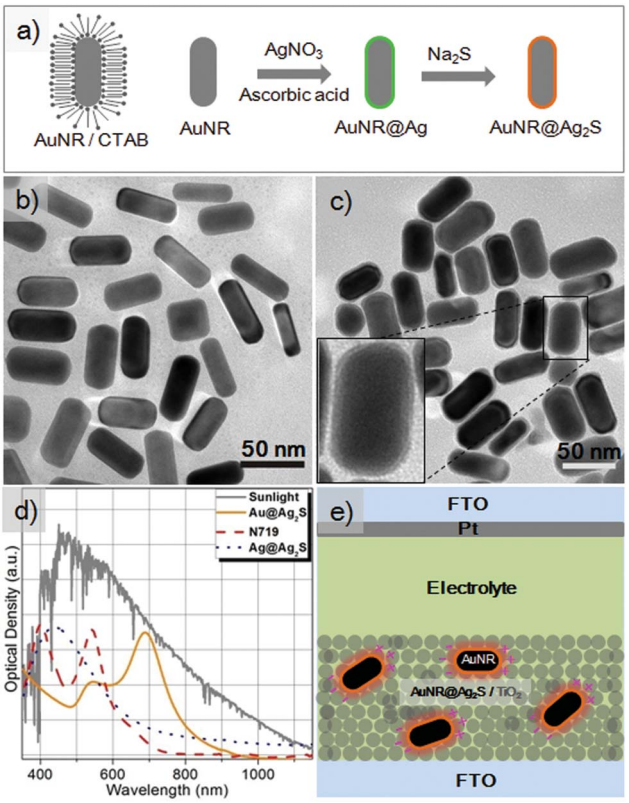

Fig. 1 A schematic illustration of a Au nanorod stabilized by hexadecyltrimethylammonium bromide (CTAB) and a two-step chemical process towards AuNR@Ag_2S (a) (CTAB is not drawn in the synthesis scheme for clarity); TEM images of as-synthesized Au nanorods (b) and AuNR@Ag_2S with Ag_2S thickness of 2 nm (c); solar irradiance spectrum, absorption of AuNR@Ag_2S (2 nm in shell thickness), N719 dye solution in acetonitrile and *t*-butanol and Ag_2S-encapsulated Ag nanoparticles, AgNP@Ag_2S (d) and a 2D device configuration of the plasmon-enhanced DSSCs, in which dye molecules were not included for clarity (e). SEM images of the TiO_2/AuNR@Ag_2S anode film are provided in the ESI.†

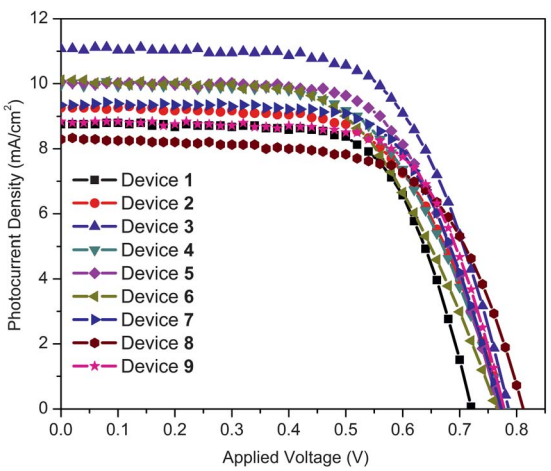

Fig. 2 The *J*–*V* characteristics of devices **1** to **9**.

equilibration between them would lead to an up-shift of the TiO_2 conduction band, thereafter enlarging the gap between the apparent Fermi level of TiO_2 and the Nernstian potential electrolyte for higher

Table 1 The J_{sc}, V_{oc}, fill factor (FF) and PCE (η) of devices **1** to **9** under one sun illumination

DSSC[a]	Anode composition[b]	J_{sc} (mA cm^{-2})	V_{oc} (V)	FF (%)	PCE (η,%)
1	TiO_2 only	8.79 ± 0.10	0.726 ± 0.018	67.1 ± 0.2	4.3 ± 0.1
2	0.88% wt Au@Ag_2S (2.0 nm)	9.28 ± 0.16	0.778 ± 0.016	62.3 ± 0.1	4.5 ± 0.1
3	1.69% wt Au@Ag_2S (2.0 nm)	11.10 ± 0.20	0.786 ± 0.006	63.7 ± 0.2	5.6 ± 0.2
4	2.05%wt Au@Ag_2S (2.0 nm)	9.99 ± 0.12	0.780 ± 0.017	60.4 ± 0.1	4.7 ± 0.2
5	1.69% wt Au@Ag_2S (3.7 nm)	10.07 ± 0.19	0.770 ± 0.022	65.1 ± 0.3	5.1 ± 0.1
6	1.69% wt Au@Ag_2S (6.0 nm)	10.64 ± 0.24	0.752 ± 0.012	56.2 ± 0.2	4.5 ± 0.1
7	Ag@Ag_2S	9.33 ± 0.15	0.772 ± 0.013	66.8 ± 0.1	4.8 ± 0.3
8	SiO_2/TiO_2-1	8.30 ± 0.16	0.812 ± 0.016	65.2 ± 0.3	4.4 ± 0.1
9	SiO_2/TiO_2-2	8.56 ± 0.18	0.779 ± 0.022	69.0 ± 0.4	4.6 ± 0.1

[a] The effective areas of all the devices are 0.24 cm^2 and the thicknesses of the anode films are 6 μm. [b] The anodes of device **2** to **6** contain different amount of AuNR@Ag_2S in TiO_2 and the anode of device **7** contains Ag@Ag_2S in TiO_2; in device **8** the concentration of SiO_2 in TiO_2 is the same as AuNR@Ag_2S in TiO_2 in device **3** and in device **9** the concentration of SiO_2 is increased by 4 times when compared with device **8**.

V_{oc}.[31,32] The substantially improved photocurrent density is attributed to the improved light harvesting (*vide infra*), which additionally contributes to photovoltage increment.[8] However, further increasing the concentration of AuNR@Ag_2S (2.05% wt, device **4**) results in a PCE decrease to 4.7%. While it is also possible that plasmon would induce electron generation at the interface and pass through the ultrathin layer of Ag_2S to the TiO_2 surface,[33,34] the contribution to the final PCE should be negligible due to the quite fast back electron transfer and low concentration of AuNR@Ag_2S.

To gain insight into the operation mechanism, the electrochemical impedance spectra (EIS) of devices **1** to **4** were characterized under open-circuit voltage and one sun illumination.[35] The equivalent circuit is depicted in the inset of Fig. 3, where R_s, R_1 and R_2 represent the series resistance and the charge transfer resistance on the counter electrode and at the interface of TiO_2/dye/electrolyte, respectively.[36,37] In an EIS spectrum, the intercept of the first circle on Z_{real}(R_s) is the Ohmic serial resistances (R_s), which is usually caused by electrolyte, electrodes and other components such as FTO, and AuNR@Ag_2S addition. Since the only difference among devices **1**–**4** is different concentrations of AuNR@Ag_2S, the increased R_s is a result of AuNR@Ag_2S addition. Owing to the conduction band of Ag_2S being higher than that of TiO_2, the high concentration of AuNR@Ag_2S existing in the TiO_2 nanoparticle network would lead to a more prominent increase in the internal electron transport resistance for the higher R_s.

The maximum frequency (ω_{max}) from the intermediate Nyquist semicircle (Fig. 3) for device **1** is 121 Hz while those of devices **2**, **3** and **4** reduce to 114, 110, and 108 Hz. Since ω_{max} is inversely associated with electron lifetime (τ_e) : $\tau_e = 1/(2\pi\omega_{max})$,[38,39] the decreased ω_{max} suggests longer electron lifetimes for PCE improvement. On the other hand, the diameters of the Nyquist semicircles correspond to charge transfer resistance (R_2) at the TiO_2/dye/electrolyte interfaces. As the conduction band of Ag_2S is higher than the LUMO of N719 (−3.85 eV *vs.* E_{vac}), an electron is unable to inject into AuNR@Ag_2S, rendering R_2s seemingly changing from 21.2, 23.6, 24.0 to 24.9 Ω for devices **1**, **2**, **3** and **4**, respectively (Fig. 3); this evolution of charge transfer resistance has a negative effect on the performance improvement. Therefore, an appropriate amount of AuNR@Ag_2S is vital for an efficient DSSC.

Further investigation is carried out to study the UV-vis-NIR absorption/transmission of the anode films. The dye-adsorbed anode film of device **1** displays the typical absorption features of N719 when compared to that of pure TiO_2 film (Fig. 4a). In AuNR@Ag_2S-incorporated films, due to the absorption of AuNR@Ag_2S ranging from 400 to 900 nm (Fig. 1d), sunlight can effectively couple with plasmon absorption in this range, which thus increases the optical

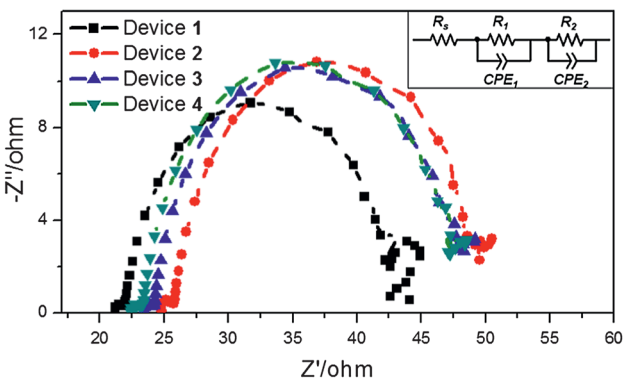

Fig. 3 Electrochemical impedance spectra of devices **1**, **2**, **3** and **4**.

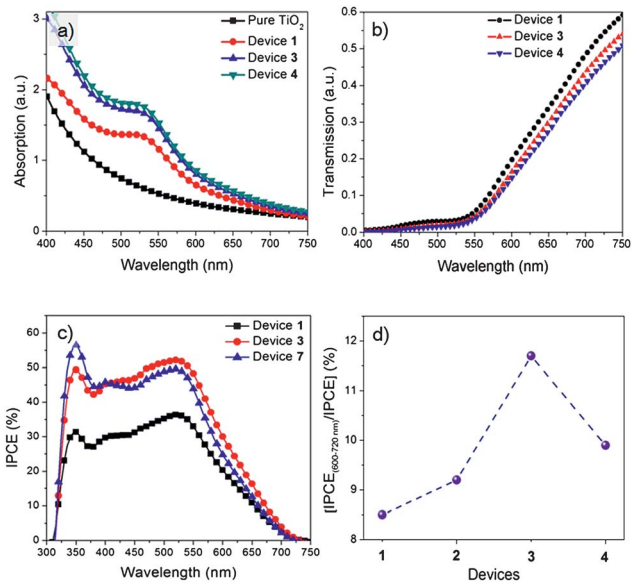

Fig. 4 UV-vis absorption and transmission spectra of TiO_2 film and anode films in devices **1**, **3** and **4** (a and b); IPCE spectra of devices **1**, **3**, and **7** (c); $IPCE_{(600-720\ nm)}$/IPCE of devices **1**, **2**, **3** and **4** (d).

density around AuNR@Ag_2S. Consequently, dye molecules placed in the vicinity of AuNR@Ag_2S usually absorb more photons.[19,32,40] In addition, the scattering effect of AuNRs would also contribute to the enhanced light utility as it can extend the optical path length. Similar phenomena have been observed in Ag nanoparticles (absorption maximum at 420 nm) enhanced DSSCs, where the whole absorption spectra of dye adsorbed films were enhanced as a result of metal nanoparticle incorporation.[19,32,40] On the other hand, transmittance spectra present a reducing trend at 600–750 nm upon the addition of AuNR@Ag_2S (Fig. 4b). The strong longitudinal SPR induced light trapping and scattering should account for the reduced transmission.[32,40] Preferably, both the increased light absorption and the reduced optical transmission are of benefit to device performance improvement.

When the thickness of the Ag_2S shell increased to 3.7 nm (device **5**), the optical absorption of the dye adsorbed anode film showed a decrement when compared with that of device **3** (Fig. S4†), indicating the space-dependent plasmonic electric field intensity.[22] The other effect of the reduced enhancement of the absorption is that, as the thickness of Ag_2S increases, the absorption maximum shifts to even longer wavelength (Fig. S5†), inducing less efficient coupling between enhanced electric field and dye molecules. As expected, when the shell thickness increased to 6.0 nm (device **6**), the optical absorption of the dye adsorbed thin film was further decreased (Fig. S4†). As a consequence, the PCEs of devices **5** and **6** decreased to 5.1% and 4.5%, respectively (Fig. 2 and Table 1).

The incident photon-to-electron conversion efficiency (IPCE) is more pertinent than UV-vis absorption/reflection for studying photocurrent generation of DSSCs. It is a product of light-harvesting efficiency, electron injection efficiency from excited dye molecules to TiO_2 nanoparticles, and electron collection efficiency at the anode. Fig. 4c shows that ICPE of device **3** is significantly improved when compared with that of device **1**. In plasmon-enhanced solar cells, plasmon excitation could improve optical density near the metal surfaces, dye molecules located in the vicinity of the nanoparticles can harvest more photons, thus increasing the IPCE.[13,19,40] For AuNR@Ag_2S, the transverse plasmon absorption at 540 nm induced light trapping could improve photocurrent generation in this region (Fig. 4c). In addition, the IPCE improvement at around 370 nm is due to the scattering effect of AuNR@Ag_2S since SiO_2 nanoparticles with comparable size could also enhance the IPCE in this range (see ESI† for details).

Notably, the IPCE of device **3** show significant broadening at 600–720 nm as compared with that of device **1** (Fig. 4c). Such broadening of the spectrum domain suggests increased light utility in this range.[7] For the reason that the film thickness of the two devices are the same and the dye loading capacity of device **1** is slightly higher than that of device **3** (Fig. S6†), the increased light utility should be promoted by the longitudinal SPR enhanced light trapping and reduced transmission (Fig. 4b).[32] To quantify the improvement, we integrate the IPCE at 600–720 nm and the whole IPCE spectra of devices **1** to **4**. The value of $IPCE_{(600–720\ nm)}$/IPCE represents the contribution from the 600–720 nm region to the overall IPCE. Calculation shows that the $IPCE_{(600–720\ nm)}$/IPCE of device **1** is 8.5%, indicating that the contribution from low energy sunlight is rather small. As a result of AuNR@Ag_2S incorporation, the values significantly change to 9.2% and 11.7% for devices **2** and **3** (Fig. 4d), clearly demonstrating the improved conversion of low energy sunlight into photocurrent. However, the IPCE at 600–720 nm of device **4** is not further increased (9.9%), but is still higher than that of device **1**. This is most likely due to decreased charge collection efficiency as a result of the increased charge transfer resistance and series resistance with high concentration of AuNR@Ag_2S as discussed above. Therefore, this preferential enhancement of IPCE in 600–720 nm manifests the AuNRs' longitudinal SPR enhanced optical density for photon-to-current conversion. In addition, our calculation shows that the conversion efficiency of light to heat due to the interband transition at longer wavelengths is smaller than that at short wavelengths (around 540 nm, Fig. S7†); this could also contribute to long wavelength sunlight harvesting in the devices.

To further verify AuNR improved low energy sunlight harvesting, we incorporate AgNP@Ag_2S into a TiO_2 anode for investigation (device **7**). The strong absorption is at 430 nm while the absorption at 600–720 nm is weak (Fig. 1d). This absorption tail results from some rod-like and non-spherical Ag nanostructures (Fig. S8†). As a result, the PCE reaches 4.8% (Table 1). The prominent improvement of the IPCE is at around 430 nm due to plasmon enhanced optical density and light scattering of AgNP@Ag_2S (Fig. 4c). However, at longer wavelength (600–720 nm) the spectral broadening is significantly smaller than that of device **3** (Fig. 4c). The correspondence between UV-vis spectra of metal nanoparticles and IPCE spectra reaffirms SPR-enhanced photocurrent generation in the DSSCs.

In DSSCs, to harvest more photons, a common method is to increase the anode film thickness in order to absorb more dye molecules. Herein we prepared DSSCs with anode films up to 11 μm using pure TiO_2, yielding a PCE of 5.8% (Fig. S9†), which is significantly improved when compared with that of device **1** (4.3%, 6 μm in film thickness). However, with only a 6 μm anode film device **3** can achieve a PCE of 5.6% (Table 1). This observation reveals that plasmon enhanced light trapping can lead to more efficient light utility. On the other hand, a thin anode film is helpful for fast carrier transport to the collecting electrode while a thick anode film unavoidably increases the electron diffusion distance. Further, when the anode is prepared using plasmonic paste with an anode thickness of 11 μm, the PCE is improved to 7.1% (Fig. S9†), indicating the effectiveness of plasmon enhanced DSSC with thicker anode films.

In summary, the use of the plasmon effect of gold nanorods is found to improve photocurrent density by efficiently converting low energy sunlight into electricity. A remarkable improvement of 37.6% in photocurrent generation at 600–720 nm is achieved. This approach to improving low energy sunlight harvesting can find wide applications due to the fact that the peak absorption of most conventional dye molecules centre at 500–600 nm. Since the optical response of gold nanorods is dependent on their aspect ratio, harvesting sunlight at various longer wavelengths can be readily achieved by simply adjusting the aspect ratio of Au nanorods. In this case, the use of plasmon enhanced light utility is complementary to the development of novel dye molecules to increase the absorption coefficient at specific wavelength regions. Finally, we believe that research aiming at improving light utility in other solar devices (such as thin film p–n junction solar cells and polymer solar cells) can also benefit from this investigation.

This work is supported by the CUHK Group Research Scheme and CUHK Focused Scheme B Grant "Center for Solar Energy Research". T. Chen is thankful for the support from RGC Research Grant (2060437). Q. LI acknowledges the support from GRF of HKSAR (Project no. 414710).

Notes and references

1 A. Hagfeldt, G. Boschloo, L. Sun, L. Kloo and H. Pettersson, *Chem. Rev.*, 2010, **110**, 6595.
2 B. Oregan and M. Grätzel, *Nature*, 1991, **353**, 737.
3 B. E. Hardin, H. J. Snaith and M. D. McGehee, *Nat. Photonics*, 2012, **6**, 162.
4 A. Yella, H.-W. Lee, H. N. Tsao, C. Yi, A. K. Chandiran, M. K. Nazeeruddin, E. W.-G. Diau, C.-Y. Yeh, S. M. Zakeeruddin and M. Grätzel, *Science*, 2011, **334**, 629.
5 T. Chen, G. H. Guai, C. Gong, W. H. Hu, J. X. Zhu, H. B. Yang, Q. Y. Yan and C. M. Li, *Energy Environ. Sci.*, 2012, **5**, 6294.
6 C. M. Lan, H. P. Wu, T. Y. Pan, C. W. Chang, W. S. Chao, C. T. Chen, C. L. Wang, C. Y. Lin and E. W. G. Diau, *Energy Environ. Sci.*, 2012, **5**, 6460.
7 A. Yella, H. W. Lee, H. N. Tsao, C. Y. Yi, A. K. Chandiran, M. K. Nazeeruddin, E. W. G. Diau, C. Y. Yeh, S. M. Zakeeruddin and M. Gräetzel, *Science*, 2011, **334**, 629.
8 T. W. Hamann, R. A. Jensen, A. B. F. Martinson, H. Van Ryswyk and J. T. Hupp, *Energy Environ. Sci.*, 2008, **1**, 66.
9 B. E. Hardin, E. T. Hoke, P. B. Armstrong, J. H. Yum, P. Comte, T. Torres, J. M. J. Frechet, M. K. Nazeeruddin, M. Gräetzel and M. D. McGehee, *Nat. Photonics*, 2009, **3**, 406.
10 Z. S. Wang, Y. Cui, K. Hara, Y. Dan-oh, C. Kasada and A. Shinpo, *Adv. Mater.*, 2007, **19**, 1138.
11 A. Burke, L. Schmidt-Mende, S. Ito and M. Grätzel, *Chem. Commun.*, 2007, 234.
12 J.-H. Yum, P. Walter, S. Huber, D. Rentsch, T. Geiger, F. Nüesch, F. De Angelis, M. Grätzel and M. K. Nazeeruddin, *J. Am. Chem. Soc.*, 2007, **129**, 10320.
13 I. K. Ding, J. Zhu, W. S. Cai, S. J. Moon, N. Cai, P. Wang, S. M. Zakeeruddin, M. Gräetzel, M. L. Brongersma, Y. Cui and M. D. McGehee, *Adv. Energy Mater.*, 2011, **1**, 52.
14 S. C. Warren and E. Thimsen, *Energy Environ. Sci.*, 2012, **5**, 5133.
15 H. A. Atwater and A. Polman, *Nat. Mater.*, 2010, **9**, 205.
16 S. Pillai, K. R. Catchpole, T. Trupke and M. A. Green, *J. Appl. Phys.*, 2007, **101**, 093105.
17 K. Nakayama, K. Tanabe and H. A. Atwater, *Appl. Phys. Lett.*, 2008, **93**, 121904.
18 X. Li, W. C. H. Choy, L. Huo, F. Xie, W. E. I. Sha, B. Ding, X. Guo, Y. Li, J. Hou, J. You and Y. Yang, *Adv. Mater.*, 2012, **24**, 3046.
19 J. Qi, X. Dang, P. T. Hammond and A. M. Belcher, *ACS Nano*, 2011, **5**, 7108.
20 W. B. Hou, P. Pavaskar, Z. W. Liu, J. Theiss, M. Aykol and S. B. Cronin, *Energy Environ. Sci.*, 2011, **4**, 4650.
21 M. D. Brown, T. Suteewong, R. S. S. Kumar, V. D'Innocenzo, A. Petrozza, M. M. Lee, U. Wiesner and H. J. Snaith, *Nano Lett.*, 2011, **11**, 438.
22 S. D. Standridge, G. C. Schatz and J. T. Hupp, *J. Am. Chem. Soc.*, 2009, **131**, 8407.
23 M. C. Daniel and D. Astruc, *Chem. Rev.*, 2004, **104**, 293.
24 X. S. Kou, S. Z. Zhang, C. K. Tsung, Z. Yang, M. H. Yeung, G. D. Stucky, L. D. Sun, J. F. Wang and C. H. Yan, *Chem.–Eur. J.*, 2007, **13**, 2929.
25 W. Ni, X. Kou, Z. Yang and J. F. Wang, *ACS Nano*, 2008, **2**, 677.
26 J. Pérez-Juste, I. Pastoriza-Santos, L. M. Liz-Marzán and P. Mulvaney, *Coord. Chem. Rev.*, 2005, **249**, 1870.
27 A. Gole and C. J. Murphy, *Langmuir*, 2008, **24**, 266.
28 M. Z. Liu and P. Guyot-Sionnest, *J. Mater. Chem.*, 2006, **16**, 3942.
29 J. Yang and J. Y. Ying, *Angew. Chem., Int. Ed.*, 2011, **50**, 4637.
30 F. Lenzmann, J. Krueger, S. Burnside, K. Brooks, M. Gräetzel, D. Gal, S. Ruhle and D. Cahen, *J. Phys. Chem. B*, 2001, **105**, 6347.
31 A. Kongkanand, R. M. Dominguez and P. V. Kamat, *Nano Lett.*, 2007, **7**, 676.
32 S. J. Lin, K. C. Lee, J. L. Wu and J. Y. Wu, *Appl. Phys. Lett.*, 2011, **99**, 043306.
33 A. Furube, L. Du, K. Hara, R. Katoh and M. Tachiya, *J. Am. Chem. Soc.*, 2007, **129**, 14852.
34 L. C. Du, A. Furube, K. Yamamoto, K. Hara, R. Katoh and M. Tachiya, *J. Phys. Chem. C*, 2009, **113**, 6454.
35 F. Fabregat-Santiago, J. Bisquert, E. Palomares, L. Otero, D. B. Kuang, S. M. Zakeeruddin and M. Grätzel, *J. Phys. Chem. C*, 2007, **111**, 6550.
36 R. Kern, R. Sastrawan, J. Ferber, R. Stangl and J. Luther, *Electrochim. Acta*, 2002, **47**, 4213.
37 N. L. Yang, J. Zhai, D. Wang, Y. S. Chen and L. Jiang, *ACS Nano*, 2010, **4**, 887.
38 C. M. Li, C. Q. Sun, S. Song, V. E. Choong, G. Maracas and X. J. Zhang, *Front. Biosci.*, 2005, **10**, 180.
39 S. R. Sun, L. Gao and Y. Q. Liu, *Appl. Phys. Lett.*, 2010, **96**, 083113.
40 B. Ding, B. J. Lee, M. J. Yang, H. S. Jung and J. K. Lee, *Adv. Energy Mater.*, 2011, **1**, 415.